processes

MDPI

Article

Experimental Study on Factors Affecting Fracture Conductivity

Fuchun Tian [1], Yunpeng Jia [1], Liyong Yang [1], Xuewei Liu [1], Xinhui Guo [2,*] and Dmitriy A. Martyushev [3,*]

[1] Petroleum Engineering Research Institute, Petrochina Dagang Oilfield Company, Tianjin 300280, China; tianfchun@petrochina.com.cn (F.T.); jiaypeng@petrochina.com.cn (Y.J.); yanglyong@petrochina.com.cn (L.Y.); dg_liuxwei@petrochina.com.cn (X.L.)
[2] College of Environment, Liaoning University, Shenyang 110036, China
[3] Department of Oil and Gas Technologies, Perm National Research Polytechnic University, Perm 614990, Russia
* Correspondence: 15537920191@163.com (X.G.); martyushevd@inbox.ru (D.A.M.)

Abstract: The conductivity of propped fractures following hydraulic fracturing is crucial in determining the success of the fracturing process. Understanding the primary factors affecting fracture conductivity and uncovering their impact patterns are essential for guiding the selection of fracturing engineering parameters. We conducted experiments to test fracture conductivity and analyzed the effects of proppant particle size, closure pressure, and fracture surface properties on conductivity. Using the orthogonal experimental method, we clarified the primary and secondary relationships of the influencing factors on conductivity. The results indicate that proppant particle size, formation closure pressure, and fracture surface properties significantly affect fracture conductivity, with the order of influence being closure pressure > fracture surface properties > proppant particle size. Using large-particle-size proppants effectively increases interparticle porosity and enhances fracture conductivity. However, large-particle-size proppants reduce the number of contact points between particles, increasing the pressure on individual particles and making them more prone to crushing, which decreases fracture conductivity. Proppants become compacted under closure pressure, leading to a reduction in fracture conductivity. Proppant particles can embed into the fracture surface under closure pressure, further impacting fracture conductivity. Compared to non-laminated fracture surfaces, proppant particles are more likely to embed into laminated fracture surfaces under closure pressure, resulting in a greater embedding depth and reduced conductivity.

Keywords: hydraulic fracturing; conductivity; proppant; closure pressure; laminated rock

Citation: Tian, F.; Jia, Y.; Yang, L.; Liu, X.; Guo, X.; Martyushev, D.A. Experimental Study on Factors Affecting Fracture Conductivity. *Processes* **2024**, *12*, 1465. https://doi.org/10.3390/pr12071465

Received: 13 June 2024
Revised: 4 July 2024
Accepted: 9 July 2024
Published: 13 July 2024

1. Introduction

Oil and gas resources are the primary energy sources globally, with increasing demand for these resources. With the increasing depths of oil and gas exploration, deep-seated reservoirs are exhibiting characteristics like tightness and low permeability [1–3]. These traits significantly constrain the augmentation of oil and gas production [4–7]. Hydraulic fracturing stands as a crucial technique for augmenting production and recovery rates in single-well operations within unconventional oil and gas reservoirs [4,8,9]. The aim of hydraulic fracturing is to establish a high-conductivity conduit linking the reservoir to the wellbore [10–13]. Proppants, along with high-pressure fracturing fluids, are injected into the fractures. They play a vital role in providing support, preventing the closure of hydraulic fractures, maintaining high conductivity, and facilitating the flow of oil and gas [14–16].

The conductivity of propped fractures directly determines the construction quality and production enhancement effects of hydraulic fracturing [17–19]. However, under high closure pressure conditions, the conductivity of propped fractures can rapidly decrease over time, with reductions of up to 95% [20,21]. Clarifying the key factors that affect fracture proppant performance and revealing their impact patterns are prerequisites for

guiding engineering parameter selection. Zhang [22] conducted conductivity tests using an improved modified American Petroleum Institute (API) conductivity cell and found that larger proppant particle sizes and higher proppant concentrations resulted in stronger proppant conductivity. Long-term conductivity tests showed that fracture conductivity could can decrease by 20% within 20 h. In addition to proppant parameters, the embedding of proppants due to high stress is also a critical factor affecting fracture conductivity. Bandara et al. [23] utilized the discrete element numerical simulation method to analyze the impact of proppant embedding. The results indicated that conventional proppants could embed to a depth of up to 88% and were prone to crushing. Wen [21] studied the influence of different proppant concentrations and types on embedding and fracture conductivity using a long-term conductivity evaluation system. The results showed that proppant embedding had a significant detrimental effect on fracture conductivity, reducing it by 87.5%. Higher proppant concentrations were found to effectively prevent the reduction in fracture conductivity. Hou [24] discovered through conductivity testing experiments that fracture conductivity was directly proportional to proppant concentration but had a more complex relationship with proppant particle size. Within the closure pressure range of 10–40 MPa, fracture conductivity was directly proportional to proppant particle size. However, at higher closure pressures, proppant particles were more prone to breakage, resulting in debris that reduced proppant porosity and blocked the flow pathways for oil and gas. Consequently, fracture conductivity was inversely proportional to proppant particle size. It can be observed that factors such as proppant particle size, closure pressure, and embedding level can all influence the conductivity of propped fractures. Furthermore, the positional relationship between fracture surfaces and joint surfaces should not be overlooked as it affects fracture conductivity. During the hydraulic fracturing process, fractures can be generated parallel or perpendicular to bedding planes. Differences in fracture surface properties can lead to variations in proppant embedding levels, thereby affecting the conductivity of propped fractures [25]. Lastly, understanding the sensitivity of conductivity to various influencing factors is of great significance in guiding the selection of engineering parameters for hydraulic fracturing [26].

Therefore, we focus on fracture conductivity and analyze the impact of proppant particle size, closure pressure, and fracture surface properties through conductivity testing experiments. The objective is to elucidate the primary and secondary relationships among factors influencing conductivity, aiming to establish a theoretical foundation for the selection of engineering parameters in hydraulic fracturing.

2. Experiment

2.1. Material

To assess the impact of proppant particle size on fracture conductivity, we conducted conductivity testing experiments utilizing quartz sand with particle sizes ranging from 106 to 212 μm (70–140 mesh), 212 to 425 μm (40–70 mesh), and 300 to 600 μm (30–50 mesh). The metal samples used exhibited significantly higher strength compared to quartz sand, rendering it challenging for the sand to embed into the metal samples under closure pressure. Consequently, we conducted experiments using both metal samples and rock samples to analyze the influence of embedding depth on fracture conductivity. Moreover, fractures may exhibit surfaces that are either vertical or parallel to bedding structures, leading to variations in fracture surface properties that influence proppant embedding and consequently alterations in fracture conductivity. We conducted conductivity testing experiments using rock samples with both vertical and horizontal bedding orientations to investigate the effects of embedding depth and bedding structures on fracture conductivity. The experimental samples were collected from the Kongdian Formation in the Cangdong Sag of the Huanghua Depression, Bohai Bay Basin. The processing and treatment of the test rock samples strictly adhered to the standard NB/T 14023-2017 [27], titled “Recommended Method for Long-term Conductivity Testing of Shale Proppant Filling Beds”. The dimen-

sions of the rock samples were as follows: length 17.75 ± 0.04 cm, width 3.75 ± 0.05 cm, and height varying between 0.9 and 1.5 cm, as depicted in Figure 1.

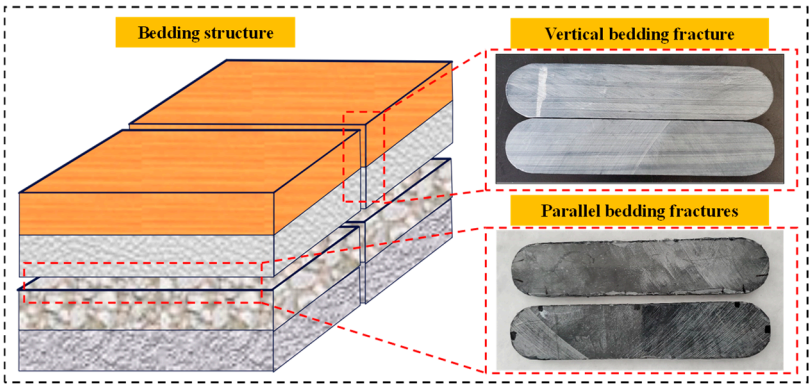

Figure 1. Vertical bedding fracture and parallel joint fracture.

2.2. Experimental Apparatus

In this experiment, the FCMS-V flow conductivity measurement system was employed to assess the flow conductivity of the propped fractures. The experimental apparatus is depicted in Figure 2a–c. The instrument can test fluid flow rates from 0 to 100 mL/min, with a maximum test pressure of 10 MPa, an operational temperature range up to 200 °C, and a maximum closure pressure of 150 MPa. The thickness of the proppant ranges from 0.25 to 1.27 cm. The measurement apparatus primarily comprises a pressure loading system and a flow conductivity testing system. The pressure loading system includes a pressure loading machine and a pressure compensation system, as depicted in the schematic diagram in Figure 2b. The hydraulic pressure sensor on the pressure machine is utilized to measure the hydraulic pressure applied, which can be converted into the load borne by the platens and the closure pressure of the proppant. The flow conductivity testing system primarily includes an advection pump, a conductivity cell, and a data acquisition control system. The conductivity cell (Figure 2c) is designed for linear flow, and the proppant placement area measures 64.5 cm^2. The design and production strictly conform to the standards of the American Petroleum Institute (API). The data acquisition control system includes differential pressure sensors, temperature sensors, displacement sensors, and more. The differential pressure sensor is employed to measure the fluid pressure difference across the proppant layer within the platens. The temperature sensor is utilized to measure the heating temperature of the platens and the intermediate container, allowing the simulation of reservoir temperature by setting the temperature manually. The displacement sensor is employed for measuring the width of the fracture.

(**a**)

Figure 2. *Cont.*

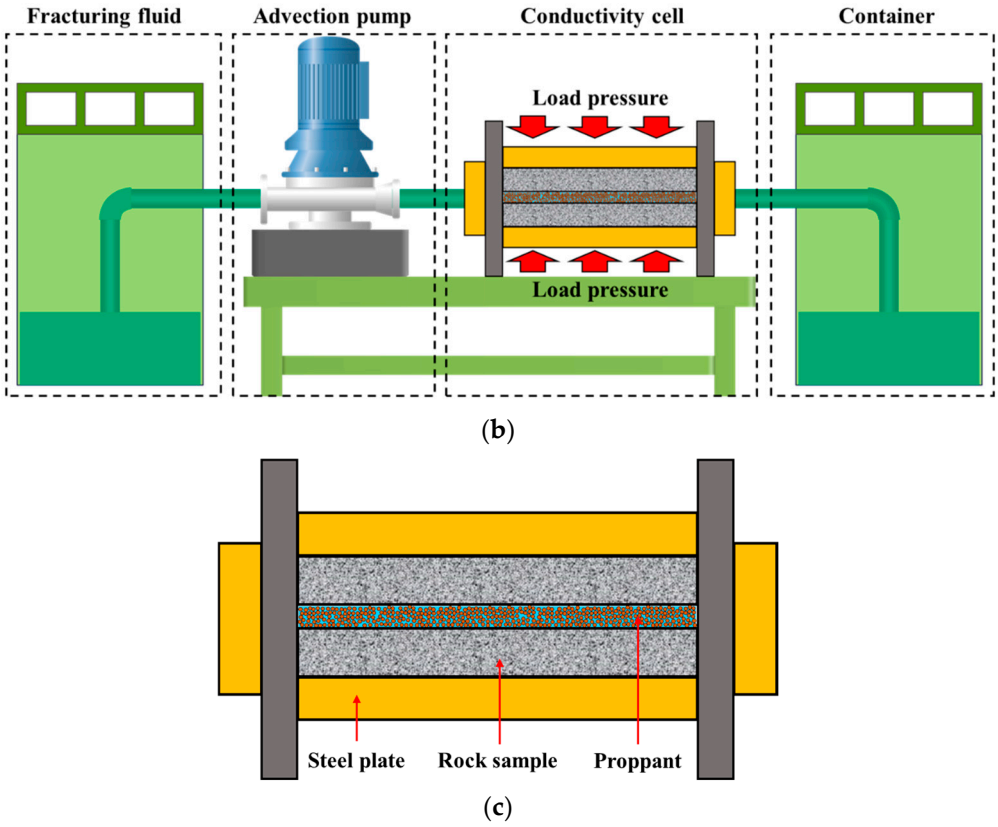

Figure 2. FCMS-V flow conductivity measurement system: (**a**) FCMS-V flow conductivity measurement experimental system; (**b**) Schematic diagram of FCMS-V flow conductivity measurement experimental system; (**c**) Conductivity cell.

After placing the rock sample into the conductivity cell, the gaps between the rock sample and the sidewalls of the conductivity cell were filled with room-temperature vulcanizing organic silicon adhesive. This step was taken to prevent the proppant from infiltrating the gaps between the rock sample and the inner walls of the conductivity cell, thus minimizing potential experimental errors. Following the placement of both upper and lower rock samples, the depths at both ends of the rock sample were meticulously adjusted to maintain a difference in depth of less than 0.1 mm.

2.3. Experimental Setup

According to the requirements of standard NB/T 14023-2017 [27], the testing duration for long-term conductivity should be within the range of 0 h to 50 h ± 2 h. To analyze the impact of proppant particle size, closure pressure, and fracture surface material on propped fracture conductivity, a series of 52 h long-term conductivity tests were conducted for each variable. The experimental schedule is elaborated in Table 1. To mitigate the impact of other variables on the experimental outcomes, proppant concentration was held constant at 10 kg/m^2, temperature at 100 °C, and flow rate at 2 mL/min.

The properties of the fracture surface can affect the depth of proppant embedding, thereby altering fracture conductivity. Therefore, following experiments 1-7 to 1-9, calculations were performed to assess the depth of proppant embedding and analyze the influence of fracture surface properties on conductivity. The determination of proppant embedment depth involves the following calculations:

(1) Assuming the rigid steel sample remains non-deformable, calculate the deformation of the crack width under various closure pressures by subtracting the initial crack width (W_{01}) from the crack width after the conductivity test (W_{02}). This calculation yields the deformation $D_0 = W_{01} - W_{02}$.

(2) In situations where the rock sample is without stratification, compute the crack deformation as $D_1 = W_{11} - W_{12}$, with W_{11} representing the initial crack width and W_{12} denoting the crack width after the conductivity test. For scenarios involving a laminated rock sample, determine the deformation of the crack width as $D_2 = W_{21} - W_{22}$, where W_{21} signifies the initial crack width, and W_{22} represents the crack width after the conductivity test.

(3) Calculate the embedment depth of the proppant as follows: for the case of non-laminated rock samples, the embedment depth is $D_{0\text{-}1} = D_1 - D_0$, and for the case of laminated rock samples, the embedment depth is $D_{0\text{-}2} = D_2 - D_0$.

Fracture conductivity is collectively influenced by a combination of various factors. To elucidate the influence of individual factors on conductivity performance, an orthogonal experimental design was employed using fracture equilibrium conductivity as the evaluation criterion. This design considered particle size, closure pressure, and fracture surface properties as variables. The levels of these three factors are presented in Table 2, and a comprehensive orthogonal experimental design is outlined in Table 3.

Table 1. Multi-factor sequential conductivity testing experiments.

Experiment Number	Particle Size (mesh)	Closure Pressure (MPa)	Fracture Surface Material
1-1	30–50	30	Steel plate
1-2	40–70		
1-3	70–140		
1-4	30–50	30	Steel plate
1-5		40	
1-6		50	
1-7	30–50	30	Steel plate
1-8			Non-laminated rock sample
1-9			Laminated rock sample

Table 2. Levels of factors in orthogonal experiment.

Levels	Particle Size (mesh)	Closure Pressure (MPa)	Fracture Surface Material
1	30–50	30	Steel plate
2	40–70	40	Non-laminated rock sample
3	70–140	50	Laminated rock sample

Table 3. Orthogonal experimental design for conductivity testing.

Experiment Number	Particle Size (mesh)	Closure Pressure (MPa)	Fracture Surface Material
2-1	30–50	30	Steel plate
2-2	30–50	40	Laminated rock sample
2-3	30–50	50	Non-laminated rock sample
2-4	40–70	30	Laminated rock sample
2-5	40–70	40	Non-laminated rock sample
2-6	40–70	50	Steel plate
2-7	70–140	30	Non-laminated rock sample
2-8	70–140	40	Steel plate
2-9	70–140	50	Laminated rock sample

2.4. Experimental Procedure

The experimental procedure consists of five main steps: the calibration of the conductivity cell, preparation of the conductivity cell, evacuation, conductivity testing, and

heating. Each step is carefully controlled to ensure the accuracy and reliability of the results. Automated systems are used to regulate pressure and temperature, and continuous monitoring is employed to detect any deviations and make real-time adjustments.

Step 1: Calibration of the conductivity cell

In conditions where no proppant is present in the conductivity cell, raise the closure pressure by 30 MPa and record the initial reading of the displacement sensor. Then, progressively elevate the closure pressure to 40 and 50 MPa while recording displacement measurements at each pressure level. These measurements form the baseline values for determining proppant fill thickness.

Step 2: Preparation of the conductivity cell

Add the specified proppant mass into the conductivity cell, followed by elevating the closure pressure to the prescribed level.

Step 3: Evacuation

Utilize a vacuum pump to remove air from the conductivity cell and connected pipes. Once the evacuation process is finished, close the valves.

Step 4: Conductivity testing

Initiate the advection pump to introduce the test medium into the conductivity cell, configuring parameters such as closure pressure, test flow rate, and pressurization duration. Automated data recording for conductivity and displacement ensues.

Step 5: Heating

Power on the heating switch and adjust to the desired temperature. The temperature controller will autonomously maintain the conductivity cell's temperature at the specified level.

3. Experimental Results and Analysis

3.1. Proppant Particle Size

Figure 3 illustrates the influence of varying proppant particle sizes on fracture conductivity at a closure pressure of 30 MPa. It is evident that with an increase in the test duration, overall fracture conductivity demonstrates a declining pattern. Initially, fracture conductivity decreases rapidly, but it gradually stabilizes with time. Furthermore, the particle size of the proppant exerts a notable influence on fracture conductivity. For particle sizes within the 30–50 mesh range, the initial fracture conductivity measures 16.3 $\mu m^2 \cdot cm$, and the stabilized conductivity is 12.25 $\mu m^2 \cdot cm$, representing a decrease of 4.05 $\mu m^2 \cdot cm$. In the case of particle sizes ranging from 40 to 70 mesh, the conductivity diminishes from 13.3 $\mu m^2 \cdot cm$ to 11.11 $\mu m^2 \cdot cm$, reflecting a decrease of 2.19 $\mu m^2 \cdot cm$. In cases where the particle size falls within the 70–140 mesh range, the initial fracture conductivity reduces from 8.64 $\mu m^2 \cdot cm$ to 6.42 $\mu m^2 \cdot cm$, resulting in a decrease of 2.22 $\mu m^2 \cdot cm$. It is evident that as the proppant particle size increases, long-term fracture conductivity improves. Nevertheless, it is important to note that the increase in proppant particle size also leads to a more pronounced reduction in the conductivity of the supported fracture under the influence of closure pressure.

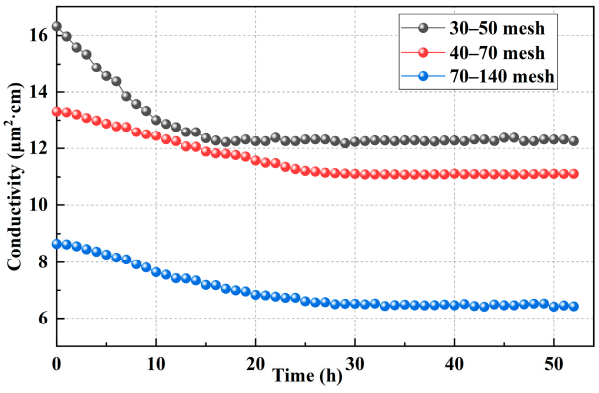

Figure 3. Effect of particle size on fracture conductivity.

During the initial phases of the experiment, the proppant experiences compaction and crushing due to the applied closure pressure [28]. Fine particles generated from the fragmentation of proppant grains are pressed together, resulting in the obstruction of pores and channels that facilitate fluid and gas transport. Consequently, this leads to a general reduction in the permeability and conductivity of the fracture. With the ongoing application of closure pressure, proppant grains undergo additional compaction, resulting in a minor decline in the overall conductivity of the fracture. Once the proppant grains attain a stable condition, their conductivity remains constant.

The utilization of larger-sized proppants effectively enhances intergranular porosity, resulting in the creation of more efficient flow pathways and consequently an improvement in fracture conductivity. Nonetheless, larger-sized support agents result in fewer contact points between particles, leading to heightened pressure on individual particles. This increased pressure facilitates support agent particles reaching their compressive strength and consequently undergoing fracture. These resulting fragments become compacted due to the impact of closure pressure, leading to a more tightly packed configuration of proppants. This, in turn, results in a swift decline in fracture conductivity. As the particle size increases, the consequences of fragmentation and compaction become increasingly prominent, resulting in a more substantial reduction in fracture conductivity. Nonetheless, enlarging the proppant particle size can still effectively enhance fracture conductivity.

3.2. Closure Pressure

Figure 4 depicts the impact of closure pressure on fracture conductivity under the condition of a particle size range of 30–50 mesh. It is evident that as the closure pressure increases, fracture conductivity consistently experiences a declining trend. At a closure pressure of 30 MPa, the initial fracture conductivity measures 16.31 μm^2·cm, and the stabilized conductivity is 12.25 μm^2·cm, representing a reduction of 24.8%. With the closure pressure increased to 40 MPa, the initial fracture conductivity decreases to 10.1 μm^2·cm, while stabilized conductivity reaches 5.56 μm^2·cm, indicating a reduction of 44.9%. Moreover, raising the closure pressure to 50 MPa leads to a decrease of 62.7% in fracture conductivity. With increasing closure pressure, the decrease in fracture conductivity becomes more significant. This phenomenon can be attributed to the rapid compaction of the porous medium created by proppant particles due to the effects of closure pressure. This leads to a reduction in the dominant flow channels and causes certain proppant particles to experience stress levels exceeding their compressive strength, leading to fragmentation. These smaller proppant fragments further obstruct transport pathways within the porous medium, resulting in a swift initial decline in fracture conductivity [29]. Higher closure pressure elevates the stress encountered by proppant particles, leading to a greater proportion of fractured proppant particles, decreased proppant porosity, and a more substantial reduction in fracture conductivity.

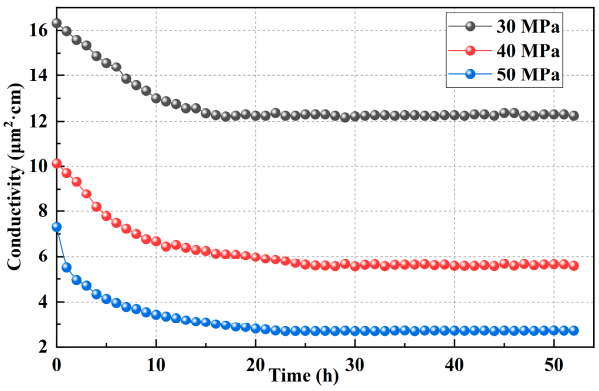

Figure 4. Effect of closure pressure on fracture conductivity.

Equilibrium conductivity is a critical parameter that determines the effectiveness of fracturing treatments. With an increase in closure pressure from 30 MPa to 40 MPa, the equilibrium conductivity decreases from 12.25 μm^2·cm to 5.56 μm^2·cm, leading to a reduction of 6.69 μm^2·cm. Furthermore, when the closure pressure is raised from 40 MPa to 50 MPa, the equilibrium conductivity decreases from 5.56 μm^2·cm to 2.72 μm^2·cm, indicating a reduction of 2.84 μm^2·cm. It is evident that augmenting the closure pressure can result in a decrease in long-term fracture conductivity. Nonetheless, as the closure pressure continues to rise, its restraining impact on fracture conductivity gradually lessens. This is because, as the closure pressure increases, the number of fractured particles gradually decreases. Furthermore, proppant particles become more densely packed, reducing the space available for the compression impact of the proppant. As a result, the inhibitory effect of closure stress on fracture conductivity gradually diminishes.

3.3. Fracture Surface Properties

Figure 5 illustrates the influence of fracture surface properties on fracture conductivity. At a closure pressure of 30 MPa and using a proppant in the 30–50 mesh size range, the utilization of steel as the fracture surface results in a long-term fracture conductivity of 12.2 μm^2·cm. Conversely, when the fracture surface consists of non-laminated rock samples, the long-term fracture conductivity measures 6.96 μm^2·cm. In scenarios where the fracture surface is composed of laminated rock samples, the long-term fracture conductivity amounts to 4.38 μm^2·cm. It is clear that variations in fracture surface properties exert a substantial influence on fracture conductivity.

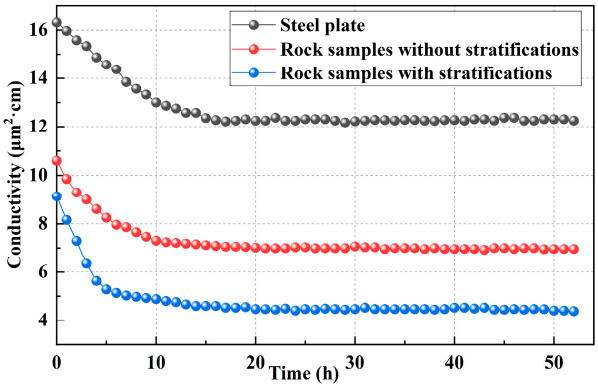

Figure 5. Effect of fracture surface properties on fracture conductivity.

To further investigate the factors contributing to the changes in fracture conductivity, electron microscopy scanning experiments were performed on the surfaces of rock samples both with and without layered structures following the experiments. The experimental results are shown in Figure 6a,b. It is evident that the proppant can become embedded within the fracture surfaces due to the effects of closure pressure. Moreover, disparities in fracture surface properties can result in differences in the extent of proppant embedment, consequently impacting fracture conductivity. Owing to the considerably higher strength of the steel sample in comparison to that of the proppant, there is minimal embedding of the proppant on the steel sample surface. In cases where non-laminated rock samples serve as the fracture surface, a portion of the proppant particles become embedded due to the influence of the closure pressure (Figure 6a). However, when experiments are carried out using laminated rock samples, the existence of layered surfaces results in a higher quantity and greater depth of proppant embedment (Figure 6b). This heightened level of proppant embedment inevitably leads to a decrease in fracture width, consequently reducing fracture conductivity [30–36].

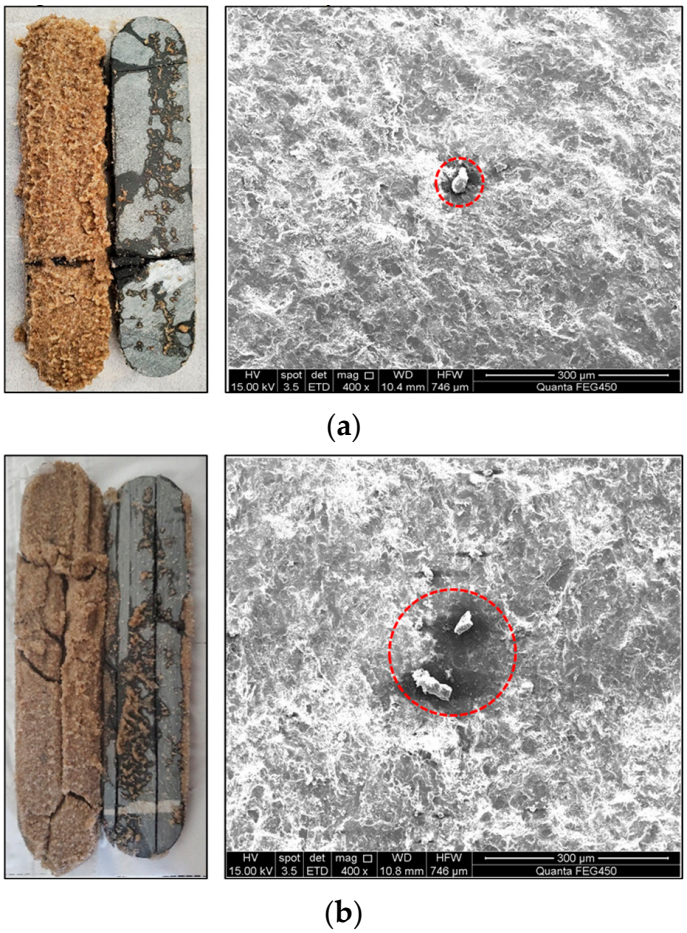

Figure 6. Electron microscopy scanning experiment results on rock samples. (The red circle in the figure indicates the proppant embedded in the rock sample): (a) Electron microscope scanning results of non-laminated rock sample; (b) Electron microscope scanning results of laminated rock sample.

Hence, in order to elucidate the impact of proppant embedment on crack width and conductivity in diverse crack surface conditions, we compared the variations in support thickness before and after conducting experiments with steel samples and rock samples. Subsequently, we calculated the depth of proppant embedment. Following this, we subtracted the equilibrium conductivity of the steel sample from that of the rock sample, both with and without bedding planes, to quantify the effect of proppant embedment on conductivity.

The impact of fracture surface properties on proppant embedment depth and conductivity is presented in Table 4 and Figure 7. The proppant embedment effect is negligible when using steel samples in these experiments. Hence, under a closure pressure of 30 MPa, the equilibrium conductivity is 12.25 $\mu m^2 \cdot cm$ in the absence of any embedment effect. For non-laminated rock samples, the embedment depth measures 0.048 mm, resulting in a decreased equilibrium conductivity of 6.96 $\mu m^2 \cdot cm$. Conversely, when employing laminated rock samples, it was observed that the embedding depth increased to 0.05 mm and the equilibrium conductivity was reduced to 6.28 $\mu m^2 \cdot cm$. It is evident that variations in fracture surface properties result in differences in proppant embedment depth, significantly impacting fracture conductivity. In contrast to non-laminated rock samples, the proppant exhibits a heightened propensity to embed within laminated rock samples under the influence of the closure pressure, ultimately resulting in a greater embedment depth. This heightened embedment depth in turn narrows the fracture width, causing a corresponding decrease in fracture conductivity.

Table 4. Embedment depths of the proppant under different fracture surface conditions.

Fracture Surface Material	Fracture Width Parameters (mm)	Value (mm)
Steel plate	W_{01}	5.724
	W_{02}	5.607
	D_0	0.117
Non-laminated rock sample	W_{11}	5.74
	W_{12}	5.575
	D_1	0.165
	$D_{0\text{-}1}$	0.048
Laminated rock sample	W_{21}	5.758
	W_{22}	5.591
	D_2	0.167
	$D_{0\text{-}2}$	0.05

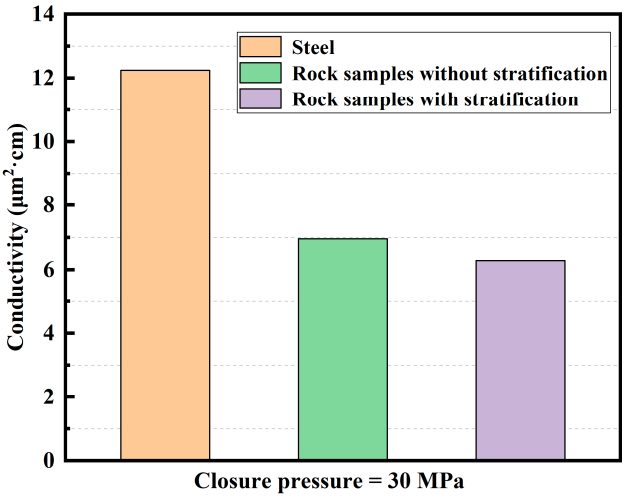

Figure 7. Fracture conductivity under different fracture surface conditions.

3.4. Analysis of Orthogonal Experimental Results

The results of the orthogonal experiments are presented in Table 5, where "R" signifies the range of each factor. The value of "R" is used to assess the impact of proppant sizes, closure pressure, and fracture surface properties on conductivity. It can be observed that the range of closure pressure is the largest, measuring 4.76 MPa. This indicates closure pressure as the primary factor impacting conductivity. The ranges for the fracture surface properties and particle sizes are relatively similar, measuring 3.639 MPa and 3.604 MPa, respectively. Hence, the order of influence on conductivity can be summarized as follows: closure pressure > fracture surface properties > particle sizes. Notably, closure pressure assumes a central role in compacting proppant particles within the fracture, thereby diminishing dominant flow pathways. This renders closure pressure the primary determinant of fracture conductivity. The fracture surface properties wield the capacity to influence the depth of proppant embedment, subsequently leading to variations in fracture width. Additionally, particle sizes can impact the porosity of the proppant layer, both of which have an impact on fracture conductivity to some extent.

Table 5. Orthogonal experimental scheme of conductivity test.

Experiment Number	Particle Size (Mesh)	Closure Pressure (MPa)	Fracture Surface Material	Conductivity (μm²·cm)
2-1	30–50	30	Steel plate	12.25
2-2	30–50	40	Laminated rock sample	3.601
2-3	30–50	50	Non-laminated rock sample	2.154

Table 5. *Cont.*

Experiment Number	Particle Size (Mesh)	Closure Pressure (MPa)	Fracture Surface Material	Conductivity ($\mu m^2 \cdot cm$)
2-4	40–70	30	Laminated rock sample	4.211
2-5	40–70	40	Non-laminated rock sample	2.273
2-6	40–70	50	Steel plate	2.5935
2-7	70–140	30	Non-laminated rock sample	3.0865
2-8	70–140	40	Steel plate	3.587
2-9	70–140	50	Laminated rock sample	0.519
K_1	18.005	19.548	18.431	
K_2	9.078	9.461	7.514	
K_3	7.193	5.267	8.331	
k_1	6.001	6.516	6.143	
k_2	3.026	3.154	2.504	
k_3	2.398	1.756	2.777	
R	3.604	4.760	3.639	

4. Conclusions

(1) The use of larger-particle-size proppants can effectively increase interparticle porosity, thereby enhancing fracture conductivity. However, larger-particle-size proppants reduce the contact points between particles, resulting in an increased individual particle load-bearing pressure and a higher likelihood of particle breakage. This leads to a denser arrangement of proppants, causing a rapid decline in fracture conductivity. As the particle size increases, the impacts of particle breakage and compaction become more pronounced, resulting in a more significant decrease in fracture conductivity. Nevertheless, increasing the particle size of proppants can still effectively enhance fracture conductivity.

(2) Higher closure pressures can initially decrease long-term fracture conductivity. Nevertheless, as the closure pressure continues to rise, the available space for proppant compaction diminishes, gradually reducing its ability to inhibit fracture conductivity.

(3) Proppant particles can embed into the fracture surface due to closure pressure, and variations in fracture surface properties can lead to differences in embedment depth, consequently impacting fracture conductivity. Compared to non-laminated rock samples, proppant particles are more likely to embed into laminated rock samples under closure pressure, resulting in a greater embedment depth.

(4) Closure pressure, fracture surface properties, and particle size can all influence fracture conductivity, with respective ranges of 4.76, 3.639, and 3.604. The order of influence of these factors on fracture conductivity is as follows: closure pressure > fracture surface properties > particle size.

(5) Due to constraints, we conducted experiments only at the laboratory scale. Future plans include conducting large-scale field experiments involving hydraulic fracturing with proppant injections to validate and analyze the experimental results.

Author Contributions: Methodology, F.T.; validation, D.A.M. and X.G.; investigation, D.A.M., X.G., and F.T.; data curation, D.A.M. and X.G.; writing—original draft preparation, F.T., L.Y., and Y.J.; writing—review and editing, F.T.; project administration, X.L.; funding acquisition, F.T. All authors have read and agreed to the published version of the manuscript.

Funding: This research was funded by the National Key Research and Development Program of China (No. 2022YFF0801204) and the Ministry of Science and Higher Education of the Russian Federation (Project No. FSNM-2024-0005).

Data Availability Statement: The raw/processed data required to reproduce the above findings cannot be shared at this time as the data also form part of an ongoing study.

Conflicts of Interest: Authors Fuchun Tian, Yunpeng Jia, Liyong Yang and Xuewei Liu were employed by the company Petrochina Dagang Oilfield Company. The remaining authors declare that the research was conducted in the absence of any commercial or financial relationships that could be construed as a potential conflict of interest.

References

1. Zou, C.; Zhu, R.; Liu, K.; Su, L.; Bai, B.; Zhang, X.; Yuan, X.; Wang, J. Tight Gas Sandstone Reservoirs in China: Characteristics and Recognition Criteria. *J. Pet. Sci. Eng.* **2012**, *88*, 82–91. [CrossRef]
2. Zhang, J. Theoretical Conductivity Analysis of Surface Modification Agent Treated Proppant. *Fuel* **2014**, *134*, 166–170. [CrossRef]
3. Gu, M.; Kulkarni, P.; Rafiee, M.; Ivarrud, E.; Mohanty, K. Optimum Fracture Conductivity for Naturally Fractured Shale and Tight Reservoirs. *SPE Prod. Oper.* **2016**, *31*, 289–299. [CrossRef]
4. Liu, Y.; Zheng, X.; Peng, X.; Zhang, Y.; Chen, H.; He, J. Influence of Natural Fractures on Propagation of Hydraulic Fractures in Tight Reservoirs during Hydraulic Fracturing. *Mar. Pet. Geol.* **2022**, *138*, 105505. [CrossRef]
5. Bolintineanu, D.S.; Rao, R.R.; Lechman, J.B.; Romero, J.A.; Jove-Colon, C.F.; Quintana, E.C.; Bauer, S.J.; Ingraham, M.D. Simulations of the Effects of Proppant Placement on the Conductivity and Mechanical Stability of Hydraulic Fractures. *Int. J. Rock Mech. Min. Sci.* **2017**, *100*, 188–198. [CrossRef]
6. Wang, X.; Zhang, X.; Zhang, M.; Zhang, Q.; Dong, P.; Ding, H.; Liu, X. Proppant Settlement and Long-Term Conductivity Calculation in Complex Fractures. *ACS Omega* **2024**, *9*, 12789–12800. [CrossRef] [PubMed]
7. Li, Y.; Peng, G.; Tang, J.; Zhang, J.; Zhao, W.; Liu, B.; Pan, Y. Thermo-Hydro-Mechanical Coupling Simulation for Fracture Propagation in CO_2 Fracturing Based on Phase-Field Model. *Energy* **2023**, *284*, 128629. [CrossRef]
8. Han, X.; Feng, F.-P.; Zhang, X.-C.; Cao, J.; Zhang, J.; Suo, Y.; Yan, Y.; Yan, M.-S. An Unequal Fracturing Stage Spacing Optimization Model for Hydraulic Fracturing That Considers Cementing Interface Integrity. *Pet. Sci.* **2023**, *20*, 2165–2186. [CrossRef]
9. Zou, J.; Jiao, Y.-Y.; Tan, F.; Lv, J.; Zhang, Q. Complex Hydraulic-Fracture-Network Propagation in a Naturally Fractured Reservoir. *Comput. Geotech.* **2021**, *135*, 104165. [CrossRef]
10. Fan, M.; Han, Y.; Gu, M.; McClure, J.; Ripepi, N.; Westman, E.; Chen, C. Investigation of the Conductivity of a Proppant Mixture Using an Experiment/Simulation-Integrated Approach. *J. Nat. Gas Sci. Eng.* **2020**, *78*, 103234. [CrossRef]
11. Cong, Z.; Li, Y.; Liu, Y.; Xiao, Y. A New Method for Calculating the Direction of Fracture Propagation by Stress Numerical Search Based on the Displacement Discontinuity Method. *Comput. Geotech.* **2021**, *140*, 104482. [CrossRef]
12. Li, Y.; Hubuqin; Zhang, J.; Yang, H.; Zeng, B.; Xiao, Y.; Liu, J. Optimization Method of Oriented Perforation Parameters Improving Uneven Fractures Initiation for Horizontal Well Fracturing. *Fuel* **2023**, *349*, 128754. [CrossRef]
13. Li, Y.; Long, M.; Zuo, L.; Li, W.; Zhao, W. Brittleness Evaluation of Coal Based on Statistical Damage and Energy Evolution Theory. *J. Pet. Sci. Eng.* **2019**, *172*, 753–763. [CrossRef]
14. Sun, H.; He, B.; Xu, H.; Zhou, F.; Zhang, M.; Li, H.; Yin, G.; Chen, S.; Xu, X.; Li, B. Experimental Investigation on the Fracture Conductivity Behavior of Quartz Sand and Ceramic Mixed Proppants. *ACS Omega* **2022**, *7*, 10243–10254. [CrossRef] [PubMed]
15. Chen, Q.; Huang, Z.; Huang, H.; Chen, Q.; Ling, X.; Xin, F.; Kong, X. An Experimental Study on the Impact of the Particle Size and Proportion of Composite Proppant on the Conductivity of Propped Fractures in Coalbed Methane Reservoirs Following Pulverized Coal Fines Infiltration. *Processes* **2023**, *11*, 2205. [CrossRef]
16. Miedzinska, D.; Poplawski, A.; Kwietniewski, M.; Lutynski, M. The Impact of CO2 Injection on Steel Balls Embedment in Shale Rock—Experimental Research. *J. Nat. Gas Sci. Eng.* **2018**, *56*, 619–628. [CrossRef]
17. Fan, M.; Li, Z.; Han, Y.; Teng, Y.; Chen, C. Experimental and Numerical Investigations of the Role of Proppant Embedment on Fracture Conductivity in Narrow Fractures. *SPE J.* **2021**, *26*, 324–341. [CrossRef]
18. Liu, Y.; Guo, J.; Jia, X.; Duan, Y.; Ma, J.; Hu, J. Long Term Conductivity of Narrow Fractures Filled with a Proppant Monolayer in Shale Gas Reservoirs. *J. Eng. Res.* **2017**, *5*, 236–249.
19. Fan, M.; McClure, J.; Han, Y.; Li, Z.; Chen, C. Interaction Between Proppant Compaction and Single-/Multiphase Flows in a Hydraulic Fracture. *SPE J.* **2018**, *23*, 1290–1303. [CrossRef]
20. Yu, J.; Wang, J.; Wang, S.; Li, Y.; Singh, A.; Rijken, P.; Elsworth, D. Conductivity Evolution in Propped Fractures During Reservoir Drawdown. *Rock Mech. Rock Eng.* **2022**, *55*, 3583–3597. [CrossRef]
21. Wen, Q.; Zhang, S.; Wang, L.; Liu, Y.; Li, X. The Effect of Proppant Embedment upon the Long-Term Conductivity of Fractures. *J. Pet. Sci. Eng.* **2007**, *55*, 221–227. [CrossRef]
22. Zhang, J.; Kamenov, A.; Zhu, D.; Hill, A.D. Laboratory Measurement of Hydraulic-Fracture Conductivities in the Barnett Shale. *SPE Prod. Oper.* **2014**, *29*, 216–227. [CrossRef]
23. Bandara, K.M.A.S.; Ranjith, P.G.; Zheng, W.; Tannant, D.D.; De Silva, V.R.S.; Rathnaweera, T.D. Grain-Scale Analysis of Proppant Crushing and Embedment Using Calibrated Discrete Element Models. *Acta Geotech.* **2022**, *17*, 4837–4864. [CrossRef]
24. Hou, T.; Zhang, S.; Ma, X.; Shao, J.; He, Y.; Lv, X.; Han, J. Experimental and Theoretical Study of Fracture Conductivity with Heterogeneous Proppant Placement. *J. Nat. Gas Sci. Eng.* **2017**, *37*, 449–461. [CrossRef]
25. Bandara, K.M.A.S.; Ranjith, P.G.; Rathnaweera, T.D. Laboratory-Scale Study on Proppant Behaviour in Unconventional Oil and Gas Reservoir Formations. *J. Nat. Gas Sci. Eng.* **2020**, *78*, 103329. [CrossRef]
26. Wang, J.; Xiong, Y.; Jiao, G.; Lei, D. Assessment of Long-Term Proppant Conductivity. *Front. Energy Res.* **2022**, *10*, 813571. [CrossRef]

27. *NB/T 14023-2017*; National Energy Administration of the People's Republic of China. Recommended Method for Long-term Conductivity Testing of Shale Proppant Filling Beds. National Energy Administration: Beijing, China, 2017.
28. Xiang, Z.; Ding, Y.; Ao, X.; Zhong, Z.; Li, Z.; Xiao, H.; Chen, Z.; Xiao, Q.; Ma, X. Experimental Study on Fracturing Fracture Deformation Mechanism of Shale Reservoir. *Front. Energy Res.* **2022**, *9*, 813978. [CrossRef]
29. Liu, Y.; Mu, S.; Guo, J.; Chen, C.; Wang, S. Model for Fracture Conductivity Considering Particle Size Distribution in a Proppant Monolayer. *J. Nat. Gas Sci. Eng.* **2021**, *95*, 104188. [CrossRef]
30. Yan, C.; Zhang, P.; Dong, L.; Zhang, C.; Cheng, Y. Long-Term Fracture Conductivity in Tight Reservoirs. *Energy Sci. Eng.* **2024**, *12*, 1187–1199. [CrossRef]
31. Martyushev, D.A.; Yang, Y.; Kazemzadeh, Y.; Wang, D.; Li, Y. Understanding the Mechanism of Hydraulic Fracturing in Naturally Fractured Carbonate Reservoirs: Microseismic Monitoring and Well Testing. *Arab. J. Sci. Eng.* **2024**, *49*, 8573–8586. [CrossRef]
32. Filippov, E.V.; Zakharov, L.A.; Martyushev, D.A.; Ponomareva, I.N. Reproduction of reservoir pressure by machine learning methods and study of its influence on the cracks formation process in hydraulic fracturing. *J. Min. Inst.* **2022**, *258*, 924–932. [CrossRef]
33. Ponomareva, I.N.; Martyushev, D.A. Evaluation of hydraulic fracturing results based on the analysis of geological field data. *Georesursy* **2020**, *22*, 8–14. [CrossRef]
34. Wang, D.-B.; Zhou, F.-J.; Li, Y.-P.; Yu, B.; Martyushev, D.; Liu, X.-F.; Wang, M.; He, C.-M.; Han, D.-X.; Sun, D.-L. Numerical simulation of fracture propagation in Russia carbonate reservoirs during refracturing. *Pet. Sci.* **2022**, *19*, 2781–2795. [CrossRef]
35. Savelev, V.V.; Ognev, I.N. Sensitivity analysis of the fracturing fluid rheology effect on the hydraulic fracture geometry in the terrigenous reservoirs. *Georesursy* **2023**, *25*, 138–148. [CrossRef]
36. SYamkin, M.A.; Safiullina, E.U.; Yamkin, A.V. Analysis of the results of modeling fluid inflow to a hydraulic fractur-ing. *Bull. Tomsk Polytech. Univ. Geo Assets Eng.* **2024**, *335*, 14–21. [CrossRef]